Accelerated carbonation of recycled concrete aggregates: Investigation on the microstructure and transport properties at cement paste and mortar scales

Farah Kaddah, Harifidy Ranaivomanana, Ouali Amiri, Emmanuel Rozière

Accelerated carbonation of recycled concrete aggregates: investigation on the microstructure and transport properties at the scale of cement paste and mortar.

Farah Kaddah[a], Harifidy Ranaivomanana[b], Ouali Amiri[c], Emmanuel Rozière[a, *]

Civil engineering and Mechanics Research Institute (GeM), UMR CNRS 6183,

[a] Ecole Centrale de Nantes, 1 rue de la Noe – 44321 Nantes, France

[b] IUT de Saint-Nazaire, 58 rue Michel Ange, 44606 Saint-Nazaire, France

[c] Polytech'Nantes, Campus Gavy, Boulevard de l'Université, 44603 Saint-Nazaire, France

[*] Corresponding author, Emmanuel.Roziere@ec-nantes.fr

Abstract

The accelerated carbonation of recycled concrete aggregates (RA) has been suggested to improve their properties. Several physical and mechanical phenomena occur during the carbonation of adhered cement mortar, but their effects are scarcely distinguished and correlated. In this study cement paste and mortar specimens have been exposed to carbonation after extended curing, and then characterized at different scales to monitor the evolution of their microstructure and macroscopic properties as a function of their carbonation degree. First the carbonation of portlandite and calcite precipitation dominate, then the carbonation of C-S-H develops with the precipitation of vaterite and the development of material stiffness. The increase in elastic modulus and carbonation shrinkage both favor microcraking: an increase in macroporosity and permeability is actually observed. Clogging effect due to the formation of calcium carbonate in the microstructure finally results in the reduction of the porosity, pore sizes, and permeability.

Keywords: Cement, Carbonation, Recycled Concrete Aggregates, Hardness, Shrinkage, Porosimetry, Permeability

1 Introduction

Huge amounts of construction and demolition wastes are generated and need to be treated with accelerated industrialization and urbanization, especially among developing countries. These regions also suffer from the depletion of natural mineral resources and the shortages of waste disposal sites. Therefore, the reuse of construction waste is imperative for saving natural resources, protecting the environment, and achieving sustainable development in the construction industry [1]-[2].

In general, recycled aggregates (RA) derived from demolished concrete consist of 65–70% of natural aggregates and 30–35% of old cement paste by volume [3]. The relative residual cement paste content of RA strongly depend on the porosity of the initial cement paste but it is not significantly affected by the crushing process [4]. Compared to the typical natural aggregates (NA) used in concrete, the adhered cement mortar on the RA has a lower density, higher porosity and water absorption and lower abrasion resistance [5] [6] [7]. Besides, the RA also contains more microcracks caused by the crushing process [8], and more interfacial transition zones (ITZ) between old cement paste and natural aggregates [9]. The concrete strength thus decreases when ~~the~~ NA are totally or partially replaced by ~~the~~ RA [8] [10]. Therefore, the use of recycled aggregates in the construction industry is limited [11] to road pavement [12] and non-structural concrete [13].

To improve the properties of the RA, several techniques have been developed and can be classified into two categories: (1) removing the attached mortar [14], (2) improving the quality of attached paste[15]. In recent years, adopting accelerated carbonation technique to improve the quality of RA has already been suggested [15],[16] [17] to densify the old cement mortar attached to the RA [18] and to enhance the physical and mechanical properties of recycled aggregates. The principle of this treatment is that CO_2 can react with the adhesive

paste on the RA, according to Equation 1 and Equation 2, to form calcium carbonate and silica gel.

$$Ca(OH)_2\ (s) + CO_2\ (g) \rightarrow CaCO_3\ (s) + H_2O(l) \qquad \textbf{Equation 1}$$

$$C_XSH_Z\ (s) + xCO_2\ (g) \rightarrow xCaCO_3\ (s) + SiO_2.tH_2O\ (s) + (z-t)H_2O\ (l) \qquad \textbf{Equation 2}$$

The solid volume of the adhesive paste is ~~higher~~ bigger after carbonation [1], which results in a higher density and a lower absorption and porosity of RA. This increase in volume does not only depends on the nature of carbonated hydrate but also on the nature of the polymorphic calcium carbonate formed [19].

Carbonation of RA improves not only their own properties and that of RA concretes but also reduces the greenhouse effect caused by the emission of carbon dioxide [8]. Using CO_2 to treat recycled aggregates actually results in CO_2 storage in the adhesive paste. In practice, under atmospheric conditions, concrete carbonation occurs but it could take more than 100 years to achieve a complete carbonation [20]. ~~It is worth noting that cement industry is one of the main sources of greenhouse gases, in particular carbon dioxide emissions [21]. Cement production generates approximately 0.8 kg of CO_2 per kg cement production, and this contributes to about 5–8 % of the global CO_2 emissions [17]. The percentage of CO_2 in cement plant fumes is approximately 15% (*i.e.* 370 times the percentage of CO_2 in the atmosphere).~~ It is therefore suitable to ensure accelerated carbonation of RA in an attempt to rapidly improve their properties (National French Project FastCarb [21]).

Almost all previous studies have focused either on the physical and mechanical properties of carbonated RA themselves [15] [22], or on the mechanical performance and durability of concrete prepared with carbonated RA [5] [8]. A significant number of studies have also focused on developing new methods to increase the efficiency of carbon dioxide sequestration: Wang et al have shown that high temperature has a significant effect on the

carbonation process [23]. Pan et al found that pretreatment with calcium hydroxide improves the efficiency of carbonation [24]. Only few studies have evaluated the impact of accelerated carbonation on the evolution of microstructure and transport properties of RA themselves. The evolution of these properties is rather complex as it results from physico-chemical and mechanical phenomena occurring at different scales, from the local environment of atoms in C-S-H to macro-cracking, the competitive effects of pores clogging which is referred to by most authors to illustrate the effect of carbonation, and those of carbonation shrinkage and the induced cracking which are poorly studied in the literature. The present study will be therefore focused on these aspects and their correlation, which constitutes the originality of this paper. Finally, it is worth specifying that due to the high variability of RA and the limited number of tests that can be performed directly on them, the experimental program will be carried out not directly at recycled concrete aggregate scale but at mortar scale representing the mortar around the natural aggregate in the recycled aggregate.

2 Materials and experimental program

2.1 Materials and samples preparation

Portland cement CEM I 52.5 from Villiers-au-Bouin, France was used in this study (Table 1). Its density was 3.13 g/cm^3 and its specific surface area was 3,900 cm^2/g.

Oxide constituents (%)									
CaO	SiO_2	Al_2O_3	MgO	Fe_2O_3	SO_3	TiO_2	K_2O	Na_2O	P_2O_3
63.70	19.60	4.50	3.90	2.30	2.60	0.20	0.70	0.13	0.20

Table 1 : Chemical composition of the used cement.

Natural siliceous sand (0-2 mm) with a specific gravity of 2.61 was used as aggregates. A purely siliceous sand was chosen for this study to be sure that observed calcium carbonate

only originates from the carbonation of the cement paste. Cement mortar was prepared with mixture proportions of cement: sand: water of 1: 2.6: 0.6.

The water-to-cement (w/c) ratio of old concretes were relatively high before the extensive use of superplasticizers, also called high-range water reducing admixtures (HRWRA). Thus a w/c ratio of 0.6 was meant to be representative of old cement-based materials crushed as RA. Moreover, a high w/c ratio was expected to accelerate the diffusion of carbon dioxide and therefore the carbonation during the experimental study.

In order to explain some of the observed phenomena, a number of additional tests must be carried out. These tests (indentation, XRD and TGA) should be performed on cement paste due to practical limitations caused by the presence of aggregates for these experiments and their analysis. As making a paste with a w/c = 0.6 causes significant segregation and bleeding, a w/c ratio of 0.4 was chosen to obtain homogeneous samples.

Cylindrical paste samples were cast in plastic molds of Ø 20×50mm. Cylindrical mortar samples were cast in molds with three different sizes of Ø 20×160mm (plastic molds), Ø 70×160mm (cardboard molds covered with plastic) and Ø 110×220mm (cardboard molds covered with plastic). Each specimen size was used to characterize the evolution of defined properties. All the samples were demolded after 24 h and then soaked in a tap water tank for 180 days at 23 ± 1 °C. This significant curing time was meant to reach high hydration degree, so that the mortar would be more representative of old mortar attached to natural aggregates in recycled concrete aggregates.

After the curing period, a preconditioning was carried out before carbonation tests. The samples were dried at 40°C for 10 days, and then stored for another 17 days in an air-conditioned room (T=20°C, relative humidity RH=55%) to homogenize the internal humidity. The temperature of 40°C was chosen to dry the material without affecting the structure of

hydration products. The purpose of such preconditioning stage was to reach a hydric state of samples close to the equilibrium with the relative humidity of the environment chosen for the carbonation stage.

Some research has been done on the natural carbonation shrinkage and this has been showed to cause the development of microcracks [25]. These microcracks were considered negligible in the case of natural carbonation [26]. In the case of accelerated carbonation, the shrinkage is faster and therefore the possibility of developing more microcracks exists. These micro cracks were actually detected on samples of paste after accelerated carbonation [27] and [28]. The comprehensive characterization of initially uncracked mortar samples allows highlighting the specific effects of accelerated carbonation and its consequences in terms of shrinkage, tensile stresses, and cracking. The mortar characterized in this study is aimed at representing the mortar around NA in the RA.

2.2 Accelerated carbonation procedure (treatment)

Before the carbonation tests, the cylindrical-shaped mortar samples were protected transversely on their bases with an adhesive tape for the medium (Ø 70×160mm) and large cylinders (Ø 110×220mm) and a layer of resin for the small cylinders (Ø 20×160mm). Then they were subjected to a two-dimensional diffusion of CO_2 in a climatic chamber connected to a CO_2 tank at 20°C, 65% relative humidity and 15% of CO_2. This humidity value was chosen from the literature as it would correspond to the optimum humidity for carbonation at 20°C [26] [29]. The concentration of CO_2 in the chamber was controlled by an automatic CO_2 regulator at 15%, which is the typical CO_2 content of exhaust gases from cement manufacturing process.

2.3 Carbonated section proportion

Each specimen size was dedicated to the characterization of specific properties. The mortar cylinders (Ø 20×160mm) were used to monitor the evolution of the composition through thermogravimetric analysis (TGA), the microstructure (SEM) ~~during carbonation~~ and ~~both carbonation depth and~~ drying shrinkage during carbonation. The mortar cylinders (Ø 70×160mm) were dedicated to the monitoring of Young's modulus during carbonation. Transport properties (gas permeability and porosity) during carbonation were measured on mortar cylinders (Ø 110×220mm). For all three sample sizes, the mass and the depth of carbonation were monitored during carbonation. The different steps through which tested specimens have gone from their mixing to carbonation test and the different characterization timelines are illustrated in Figure 1. As the carbonation of small cylinders is much faster than that of medium and large cylinders, different timelines have been set as shown in Figure 1 in order to monitor the evolution of each size during the carbonation.

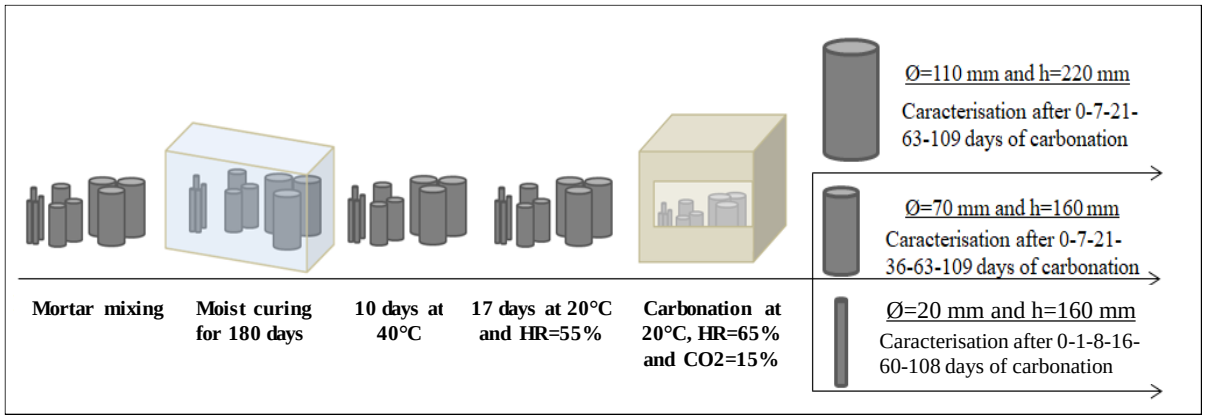

Figure 1 : Schematic drawing of experiment procedure

In order to correlate all the results obtained on samples of different sizes and given that carbonation is bidirectional in the present study, the parameter chosen to represent the carbonation progression was the ratio between the carbonated cross-sectional area and the

155 total cross-sectional area (Equation 3). The carbonated depth was determined using
156 phenolphthalein (Figure 2).

$$\text{Carbonated section proportion (CSP)} = \frac{\pi*(Ø^2-(Ø-2*d)^2)}{\pi*Ø^2} * 100 \qquad \textbf{Equation 3}$$

157 *d* is the carbonated depth determined using phenolphthalein test.

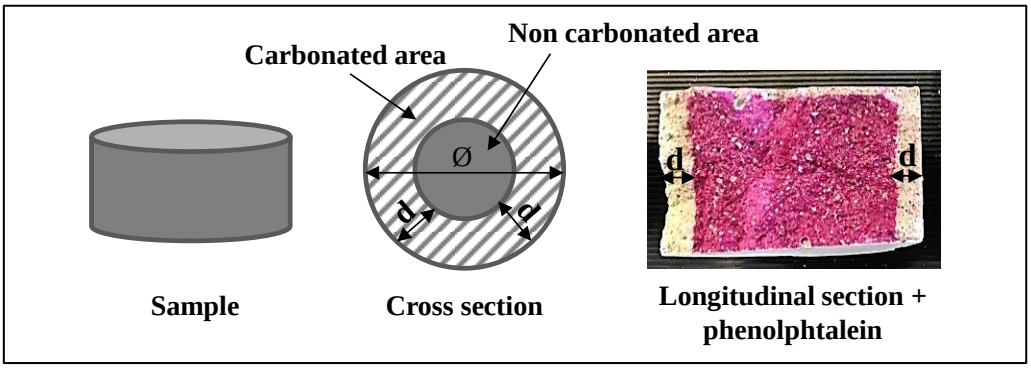

158

159 **Figure 2 : Schematic drawing of CSP determination**

160 2.4 Thermogravimetric analysis (TGA)

161 The thermal analysis was performed using a NETZSCH microbalance. A 2 cm thick sample
162 was crushed and sieved. The resulting powder sample, with a mass around 120 mg, is
163 collected in an alumina crucible and placed in the thermal balance. The tests were performed
164 under a nitrogen stream in the temperature range from 20 to 1000°C with a heating rate of
165 10°C per minute. Samples of paste and mortar were tested by TGA during their carbonation.
166 The tests performed on the paste were used to correlate the TGA results with the
167 microindentation and XRD results, while the tests performed on the mortar were used to
168 correlate the TGA results with the results of transport properties, carbonation shrinkage and
169 modulus of elasticity. Figure 3 shows an example of the TGA and derivative (DTG) curves
170 obtained.

171

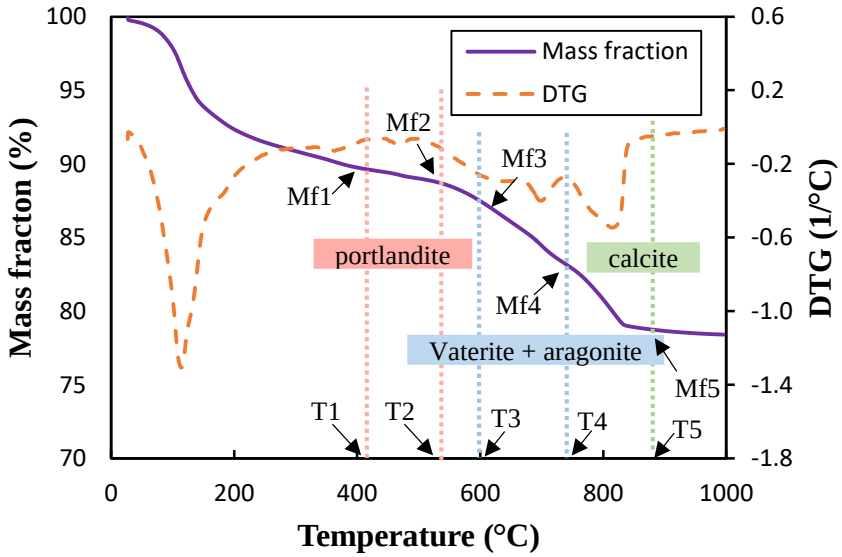

Figure 3 : Treatment type model of thermogravimetric analysis curves

~~The graph also provides the different limit temperatures used for the identification of crystallized phases. The exact boundaries temperatures were determined using the derivative curves, basing on several guidelines~~ [29] ~~–~~[30]~~.~~ Many authors have identified the decomposition temperature ranges of the phases of cement-based materials [29] [30]. These temperatures are likely to vary as a function of measurement parameters (heating rate, number of measuring heads, type of sample holder) or the sample.(compactness, mass, **carbonation rate**) [31] [32] [33]. Therefore, in this study, the limit temperatures Ti are clearly defined by the edges of the characteristic peaks of the DTG curve [26] [33] [34] (Figure 3).

The contents of portlandite CH, vaterite + aragonite, and calcite (percentage by mass in the sieved mortar) are calculated on the basis of Equation 4, Equation 5 and Equation 6 respectively.

$$CH = (M_{CH}/M_{H2O})\cdot(Mf1-Mf2) \quad \textbf{Equation 4}$$

$$\text{Vaterite+aragonite} = (M_{CaCO3}/M_{CO2})\cdot(Mf3-Mf4) \quad \textbf{Equation 5}$$

$$\text{Calcite} = (M_{CaCO3}/M_{CO2})\cdot(Mf4-Mf5) \quad \textbf{Equation 6}$$

Where Mfi is the mass fraction corresponding to the limit temperatures Ti determined using the DTG curve as mentined above (Figure 3). M_{CH}, M_{H2O}, M_{CO2} and M_{CaCO3} are respectively the molar mass of $Ca(OH)_2$, H_2O, CO_2, and $CaCO_3$ (M_{CH}=73g/mol; M_{H2O}=18g/mol; M_{CO2}=44g /mol; M_{CaCO3}=100 g/mol).

2.5 Measurement of shrinkage

2.5.1 Drying and carbonation shrinkage:

The shrinkage of the mortar was measured on cylindrical samples with a diameter of 20 mm and a height of 160 mm. The samples were equipped with metal studs placed in the mold at each end before casting. These studs made it possible to place the cylinder in a vertical sensor to measure the longitudinal deformation with a precision of 0.02 mm. ~~which allowed the cylinders to be placed in the vertical sensor with a precision of 0.02mm.~~ The measurements ~~longitudinal deformation~~ were automatically ~~measured~~ recorded using the USB-ITPACK software.

After the 180-day curing, the shrinkage was measured during preconditioning step (10 days at 40°C and 17 days at 20°C, see section 2.1). Then shrinkage was measured during the carbonation stage in the carbonation chamber (T = 20 °C, % CO_2 = 15% and RH = 65%) and the air-conditioned room (T = 20 °C, % CO_2 = 0.04% and RH = 55%). Shrinkage measurements were recorded continuously for 3 months of carbonation.

2.6 Transport properties measurements

2.6.1 Porosity accessible to water

Total porosity (i.e. the volumetric proportion of voids) was determined under vacuum according to the French standard NF P18-459. The slices were placed in a desiccator under vacuum for 4 hours (± 30 min), then the desiccator was filled with water for 44 hours (± 30 min). The slices were then dried at 105°C to constant weight. The following weights were recorded:

- W_{dry}: dry weight of the sample, after oven-drying at 105°C.
- W_{sat}: weight in air of saturated-dry surface sample.
- W_{hydro}: hydrostatic weight, weight in water of saturated sample.

The total porosity is then obtained from the following Equation 7:

$$\text{Porosity (\%)} = \frac{Wsat - Wdry}{Wsat - Whydro} * 100 \qquad \textbf{Equation 7}$$

The test was carried out at each characterization time on two samples (Ø=110mm; h = 3cm). The samples were sawn from two different cylinders.

2.6.2 Mercury intrusion porosimetry

Carbonation modifies the total porosity and the pore size distribution of cement-based materials. Pore sizes have a direct influence on transport properties such as permeability [35]. For that purpose, a standard porosimeter which allows the application of pressures up to 400 MPa has been used. This corresponds to a minimum pore radius of 1.5nm. Assuming that pores are cylindrical, the radius r, penetrated by mercury at pressure P, can be calculated by the Washburn Equation 8:

$$r = \frac{2*\sigma*COS(\theta)}{P}$$ **Equation 8**

with σ the surface tension of the mercury (σ = 0.475 N / m) and θ the contact angle between the solid surface and the mercury (θ = 141°).

Mercury intrusion porosimetry was performed on small pieces of mortar (3 to 5 mm) dried in an air-conditioned room at 20°C and 50% RH for 24 hours before the test. Those latter were taken from the carbonated and non-carbonated zone for two different carbonated section proportion (CSP=15% and CSP= 55%).

2.6.3 Gas permeability

The test consists in applying a constant pressure gradient to a sample (Ø=110 mm; h=50 mm) and measuring the gas flow through the sample at equilibrium. 2 samples were tested at each stage. It is then possible to calculate the apparent permeability which depends on the applied overpressure. The test was carried out at overpressures of 1bar, 1.6 bar, 2 bar and 2.4 bar.

The apparent and intrinsic permeabilities were measured after 7 days (K7) and 28 days (K28) of drying at 80°C and after a total drying at 105°C (Kdry). At each characterization time, 2 samples were tested. Samples were sawn from two different cylinders of the same size. For each sample and each pressure the apparent permeability was calculated from Equation 9.

$$Ka = \frac{Q1*2*\mu*L*Patm}{S(P_1^2 - P_{atm}^2)}$$ **Equation 9**

Q1: volume flow at the inlet (m^3/s)

μ: dynamic viscosity of nitrogen (Pa.s)

P_1: injection pressure (Pa)

Patm: atmospheric pressure (Pa)

L: thickness of the sample (m)

S: section of the sample (m^2).

From the apparent permeability measurements the intrinsic Kv permeability can be deduced according to Klinkenberg's approach (1941) (Equation 10).

$$K_a = K_V\left(1 + \frac{\beta}{P_m}\right) \qquad \textbf{Equation 10}$$

P_m: Mean pressure, equal to (P_1 + Patm) / 2

β: Klinkenberg's coefficient.

2.7 Mechanical properties

2.7.1 Elastic modulus

The static modulus of elasticity (E) of mortar was assessed on the cylindrical specimens (Ø=70 ×140mm) in accordance with the ASTM C 469-65 at different carbonation rates. The average of 3 values was considered at each characterization time.

2.7.2 Microhardness

In a microindentation test, a diamond indenter of specific geometry is impressed into the surface of the samples using a known applied load. The microindenter monitors and records the load and the displacement of the indenter and provides an indentation load–depth curve. The indentation load at the peak indentation depth can be used as a manifestation of the surface hardening of the samples.

In this study, a Fischer digital microhardness tester (FISCHERSCOPE HM2000) was used to measure the microhardness at the surface of the paste sample at each characterization. The microindentation test was carried out on paste instead of mortar to avoid the effect of sand particles. The 20mm thick paste sample was first finely polished to meet the experimental requirements of the digital microhardness tester.

The indenter was initially at the center of the cylindrical sample (abscissa X=0mm) and then moved towards the edge of the sample (abscissa X=10mm). On this 10mm linear path, 102 indentations were performed. At each indentation a force of 300 N was imposed for 10s and the value of the depth reached by the indenter was used to characterize the hardness of the sample at this point.

2.8 X-Ray diffraction

XRD analyses were carried out on a Malvern Panalytical Aeris instrument. It combines two technologies from Aeris and Zetium and provides full material characterization by adding information about elemental composition determined by Zetium to the phase identification from Aeris.

Scanning program consisted in rotating between 7 and 70°2θ with a step size of 0.01°2θ and a time per step of 480.165 ms.

XRD analysis was performed on paste instead of mortar to avoid the effect of sand particles, as many peaks associated to quartz sand would have appeared in results. The measurements were carried out on three samples at different stages of carbonation: before carbonation, after 3 days of carbonation and after 6 days of carbonation.

2.9 Microstructural observation

The morphologies of the representative mortar before and during accelerated carbonation were observed via a scanning electron microscopy with energy dispersive X-ray spectroscopy (SEM-EDX).

For each observation, a 2cm thick sample was put in the resin for 48 hours. Then the surface of the sample was polished and covered with a gold layer before SEM observations in order to

obtain clear images and to facilitate the identification of the different components present and formed during carbonation.

3 Results and discussion

3.1 Microstructure and properties of formed phases

3.1.1 Thermogravimetric analysis

Figure 4 shows the results of analyses performed on samples of mortar at different carbonation times in terms of carbonated section proportion (CSP). For uncarbonated samples (CSP=0%), two negative peaks can be distinguished after 200°C. These are related to the decomposition of portlandite CH (around 450-550◦C [36]) and calcium carbonate (around 550-950°C [37]). ~~$CaCO_3$~~ Calcite was present, in a small amount, in raw samples, because of the usual reaction of cement pastes with atmospheric CO_2 prior to the carbonation treatment.

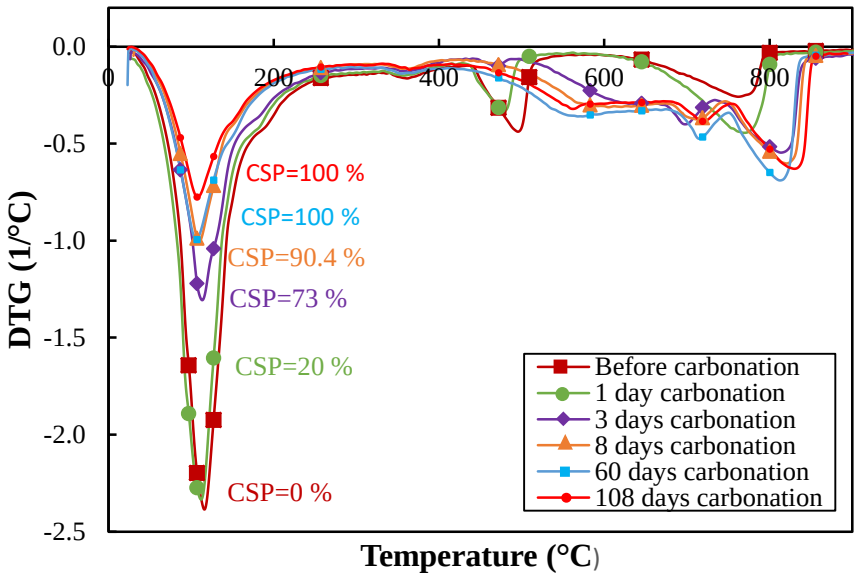

Figure 4 : Thermogravimetric analysis curves (DTG) of carbonated mortar at different carbonation ages.

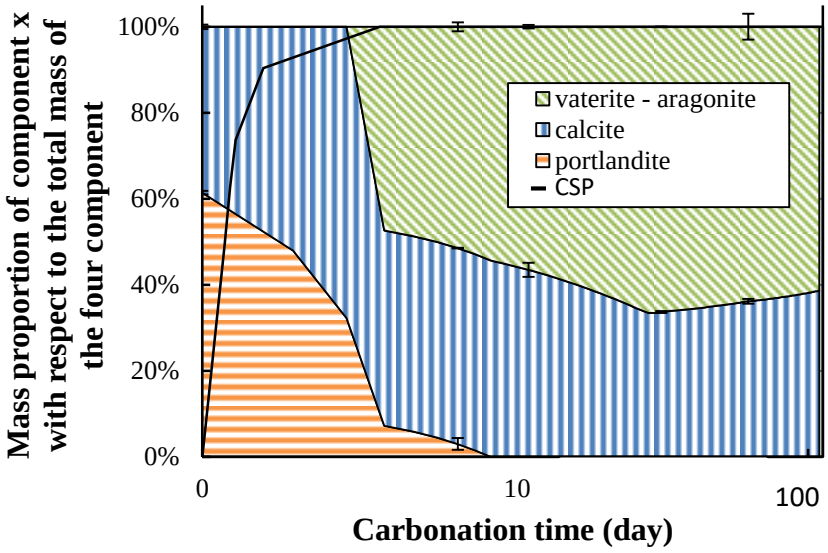

Figure 5 : Carbonation of mortar: Evolution of the mass distribution of the four components (calcite, portlandite, vaterite, and aragonite) with respect to the total mass = mass of calcite + mass of portlandite + mass of aragonite + mass of vaterite

As the carbonation progressed (CSP increase), it is noteworthy that the portlandite peak rapidly decreased ~~so that it completely~~ and completely disappeared after 8 days of carbonation (CSP=90.4%) while the peak of ~~calcium carbonate~~ calcite significantly increased at the same time. Precipitated calcite particles can be detected by SEM after 1 day of carbonation (Figure 6-b). After the first 8 days the amount of calcite (Figure 5) remained almost constant as the carbonation progressed while two new peaks corresponding to the other two polymorphs of calcium carbonate: vaterite and aragonite developed (Figure 4) [29].[34] The more the carbonation advanced, the larger these peaks and the wider the mass loss temperature range became.

The type of calcium carbonate polymorph formed depends on the type of hydrates affected by carbonation and consequently on the pH of the pore solution. The carbonation of portlandite initially dominates. As long as Portlandite ~~has~~ is not ~~fully~~ completly dissolved, it maintains a basic pH of the interstitial solution around 12.5 due to its important buffering effect [26]. At

this stage of carbonation, calcite – the stable polymorph of calcium carbonate – is the dominant polymorph formed during carbonation [38] [39] as seen in Figure 4 and Figure 5. Its decarbonation took place between 720 and 960°C [36]. As carbonation progresses, portlandite is depleted and the remaining particles are covered by calcite crystals. As a result, its carbonation becomes very slow compared to other hydrates, especially C-S-H [23]. However, since C-S-H have no buffering effect, their carbonation induces a decrease in the pH of pore solution to lower than 9 [40]. The formation of other polymorphs (vaterite, aragonite) becomes therefore predominant [41] as seen in Figure 5 after almost 8 days of carbonation. These two polymorphs decompose between 550 and 720°C (Figure 4) which suggests a poorly-crystalline [36] and less stable [42] phase.

The formation of vaterite is more pronounced than aragonite during the carbonation of CSH [38]. This is confirmed by TGA results and SEM observations. Figure 6 after 16 and 60 days of carbonation shows the significant precipitation of vaterite. In fact, vaterite has no distinct morphology, in agreement with the literature data [43] [44]; its formation occurs as sub-µm-sized spherical particles as seen in Figure 6-c. The detection of aragonite which have needle-shaped crystal morphology [43] [44] was difficult on all the images obtained. ~~Concerning TGA results the aragonite peak was observed after 109 days of carbonation (figure 4) (between 500 and 600°C).~~

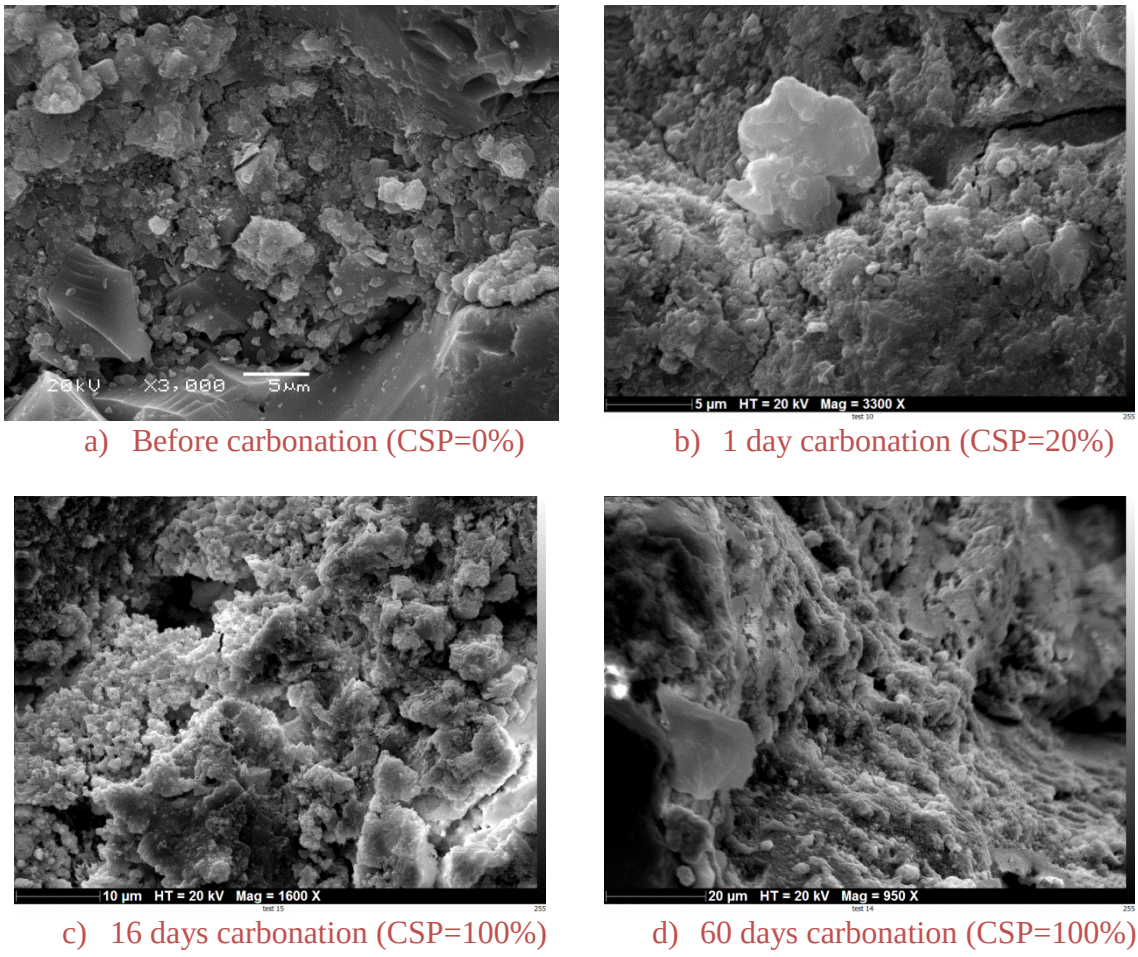

a) Before carbonation (CSP=0%) b) 1 day carbonation (CSP=20%)

c) 16 days carbonation (CSP=100%) d) 60 days carbonation (CSP=100%)

Figure 6 : SEM images after different carbonation ages.

The last observation concerns the temperature limits. It was not possible to establish a precise temperature, which limits the temperature range of the portlandite decomposition and calcium carbonate precipitation [33]. It is noteworthy to mention that these temperatures are not fixed for each component, especially for calcium carbonate and, moreover, the corresponding peak is shifted as the carbonation proceeds. This aspect, illustrated in Figure 4 ~~for calcite, aragonite and vaterite peaks,~~ can be explained by the particle size of the calcium carbonate ~~that is influenced by the thermal dissociation of calcium carbonate [33].~~ As carbonation advances, the particles of calcium carbonate become denser and therefore their dissociation temperature increases [33].

3.1.2 Microhardness

The micro indentation test was carried out on paste as already indicated to avoid the effect of sand particles. Figure 7 shows the change in hardness as a function of the distance from the center of the polished cylinder after three carbonation times: before carbonation, after 3 days and 6 days of accelerated carbonation. In order to understand its evolution, DRX (Figure 8) and TGA (Figure 9) tests were carried out on paste at the same time of carbonation as of microindentation. The dotted lines on the curves represent the boundary between the carbonated area and the non-carbonated area detected by the phenolphthalein indicator on paste specimens.

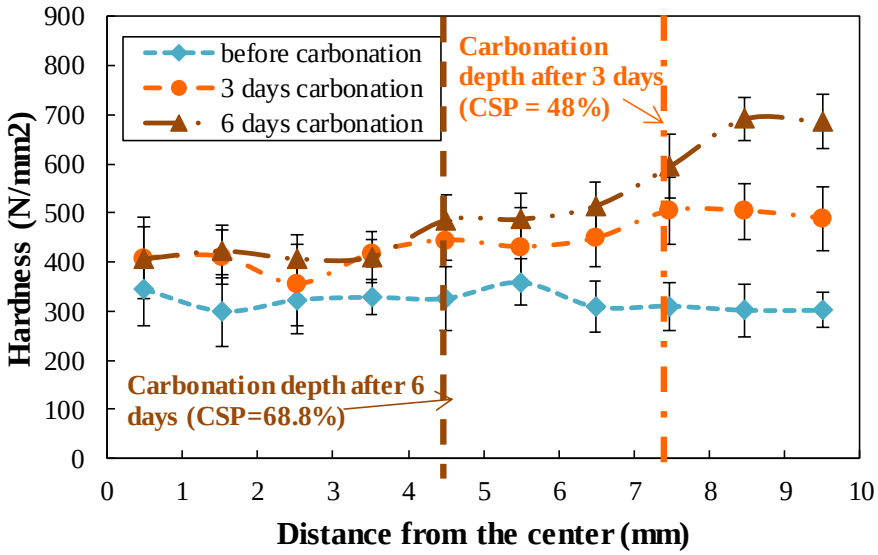

Figure 7 : Evolution of the microhardness of the cement paste during carbonation

The first curve corresponds to the hardness before carbonation of a sample along the radius (from center: X = 0 mm to edge: X = 10 mm). The value of hardness is constant with a very small reduction at the edge due to an edge effect. The second curve obtained after 3 days of carbonation shows a gradual increase from the center to the edge. The hardness of the carbonated zone detected by phenolphthalein (dotted line on the graph X = 7.4mm) has undergone the greatest increase. It is noteworthy that the zone where hardness significantly

363 increased was larger than the zone with low pH ~~as indicated~~ detected by phenolphthalein. The
364 third curve obtained after 6 days of carbonation reveals a strong increase in the hardness at the
365 edge. At the center, hardness did not significantly increase from 3 days to 6 days. The fact
366 that the carbonated zone detected by phenolphthalein (dotted line on the graph X = 4.7mm)
367 undergoes the greatest increase is in agreement with the curve obtained after 3 days of
368 carbonation. It has been observed that the measured microhardness of the cement pastes in the
369 carbonated zone, was higher than that of the non-carbonated [45]. As the carbonation
370 progresses, the evolution of the composition of the paste (Figure 8 and Figure 9) and
371 consequently the physicochemical properties of the cementitious material causes a
372 modification at the level of the microstructure of cement paste [46] [47] [48] [49]. These
373 microstructural changes help to discuss the evolutions of mortar properties that were
374 monitored in this study such as the transport properties [46] [47] and mechanical properties
375 [46]. The improvement of mechanical properties in carbonated area could be expected [46]
376 and this is consistent with the significant calcium carbonate formation after 3 and 6 days of
377 carbonation shown in Figure 9. Such precipitation, concentrated at the edge of the paste
378 sample [26] [29], is responsible for the clogging of the pores and the healing of the cracks that
379 increase the hardness of the concerned area.

380 Figure 8 also shows that calcium carbonate precipitates into different polymorphs. However,
381 the precipitation of these polymorphs is not simultaneous. After 3 days, calcium carbonate is
382 mainly formed as calcite (2Θ = 29.4 and 39.4 [37]) whereas after 6 days vaterite and aragonite
383 are also present. These results are in consistent with the results of DTG analysis in Figure 9,
384 the two peaks which appear after 6 days of carbonation between 550°C and 720°C correspond
385 to the precipitation of the poorly crystallized $CaCO_3$ as vaterite and aragonite ~~from the~~
386 ~~carbonation of C-S-H~~ [37].

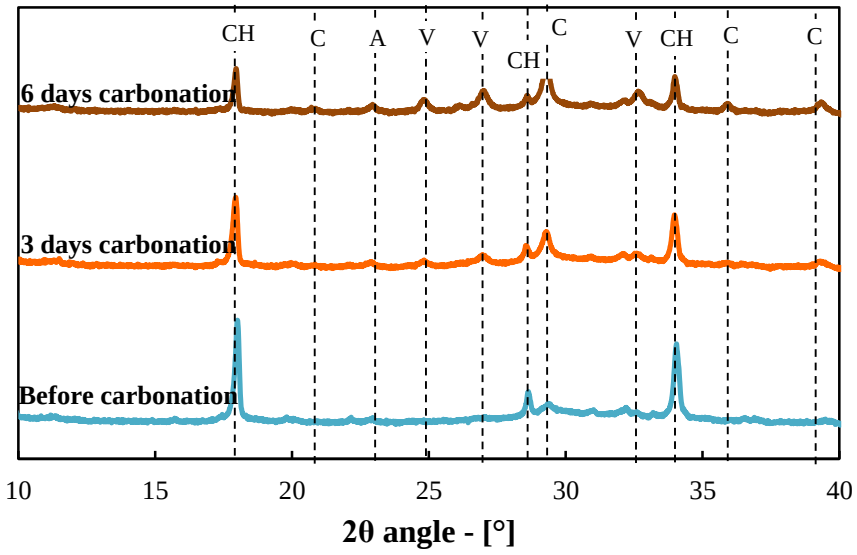

387

388 **Figure 8 : XRD of paste during carbonation**

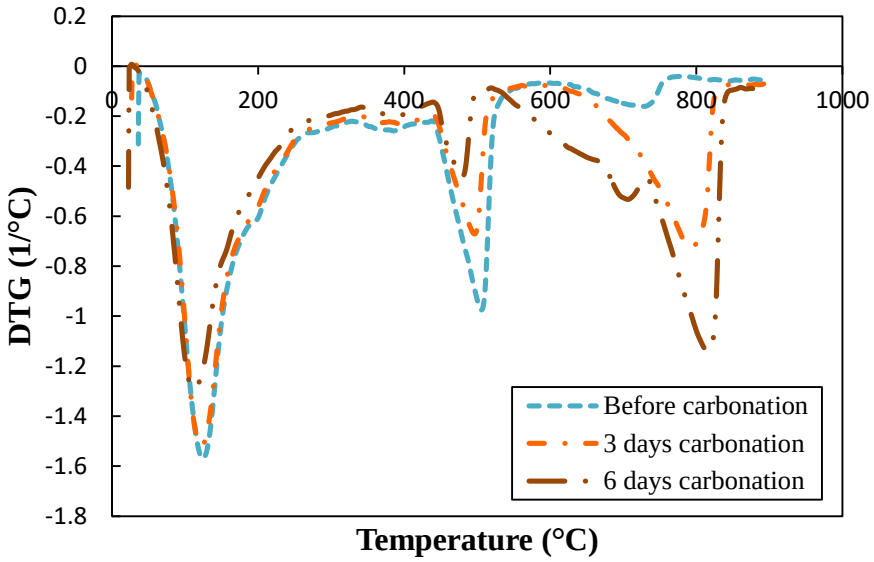

389

390 **Figure 9 : DTG of paste during carbonation**

391 It is worth noting that polymorphs of calcium carbonate have different hardness and elastic
392 modulus [43]. Vaterite has the highest hardness and elastic modulus (elastic modulus E found
393 to be in the ranges of 16 to 61 GPa), then calcite (E found to be in the ranges of 6 to 41GPa)
394 and finally aragonite (E found to be in the ranges of 2 to 34 GPa) [43]. The effect of this
395 difference in hardness and elastic modulus between the polymorphs appears on the curve

obtained after 6 days of carbonation in Figure 7. The significant increase in the hardness of the carbonated zone after 6 days of carbonation can be explained by the formation of vaterite detected by TGA, which exhibits higher value of hardness compared to the calcite formed after 3 days of carbonation.

Negative effects of the increase in hardness can also be pointed out. The carbonated zone actually becomes more vulnerable to stress-inducing phenomena such as drying and more brittle and thus more sensitive to the propagation of cracks [28] [50]. On the other hand, the existence of two separated zones having different elastic modulus in a not fully carbonated surface, can also induce the development of tensile stresses between the surface and the core of the sample. Consequently, cracks or microcracks may be generated. The development of tensile stresses is not constant during the carbonation. Due to structural effect, it initially has low values before increasing until reaching a peak and decreasing after stress relaxation due to cracking and ~~finally due to a~~ complete carbonation of the specimen.

3.2 Macroscopic properties and time-dependent behaviour

3.2.1 Mass gain and carbonation rate

Figure 10 shows the evolution of the mass of the three sample sizes during carbonation. The mass increase is calculated from Equation 11.

$$\text{Mass increase (t)} = \frac{mass\ after\ carbonation\ of\ time\ t\ -\ mass\ before\ carbonation}{mass\ before\ carbonation} \qquad \textbf{Equation 11}$$

The increase in mass observed was very pronounced at the initial stage of carbonation than it became slower. The stabilization period depends on the size of the samples. This stabilization was faster when the sample size was smaller. It began after 8 days for small cylinders (Ø=20mm; h=160mm), 60 days for medium-sized cylinders (Ø=70mm; h=160mm), while for large cylinders (Ø=110mm h=220mm) the mass was still increasing after 110 days.

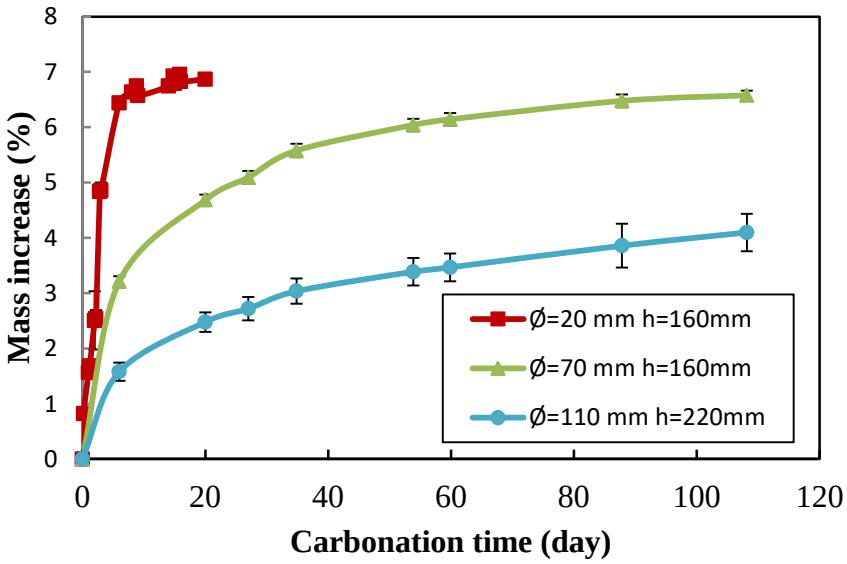

418

419 **Figure 10 : Mass gain during carbonation as a function of carbonation time**

420 To relate the results of tests carried out on samples of different sizes, the carbonated section
421 proportion was defined (see section 2.3). Figure 11 shows the evolution of the mass of
422 samples of different sizes as a function of the carbonated section proportion.

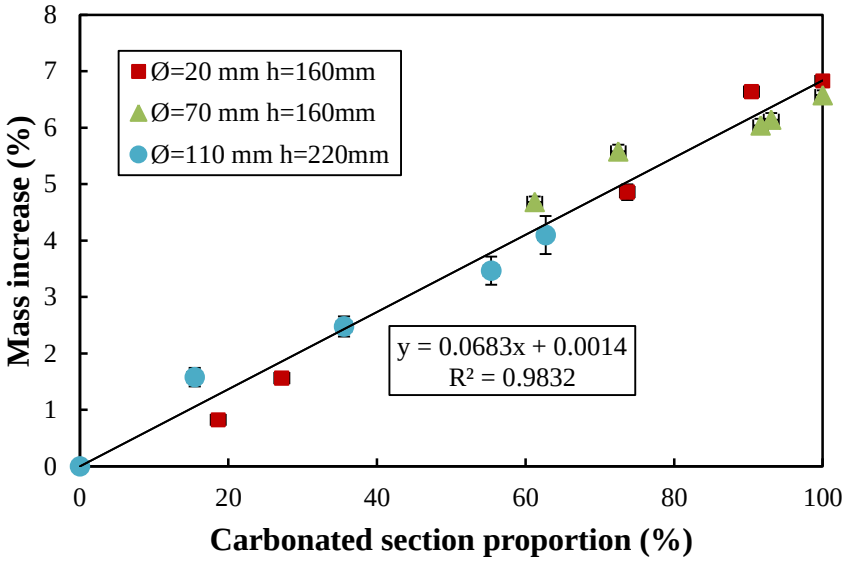

423

424 **Figure 11 : Mass gain as a function of the carbonated section proportion**

425 With respect to this parameter, the mass increase curves of the samples of different sizes ~~are~~
426 ~~very close and~~ follow the same linear increase (Figure 11). This validates the possibility of

using the carbonated section proportion defined in previous section as an indicator of the progress of physico-chemical transformation to be correlated to the evolution of other properties regardless of the size of the sample.

3.2.2 Shrinkage of mortar during carbonation

Figure 12 displays both drying and carbonation shrinkage that occur during the preconditioning step and carbonation tests respectively.

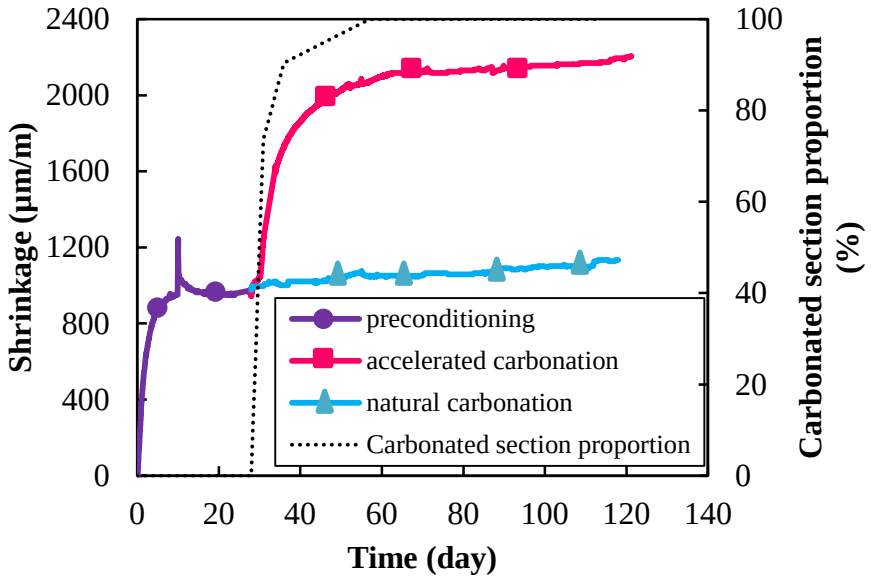

Figure 12 : Shrinkage of mortar during preconditionning and carbonation

The shrinkage during the first 27 days corresponds to the drying shrinkage associated to the preconditioning. After preconditioning, the bottom curve corresponds to the shrinkage of the sample placed in the air-conditioned room and undergoing natural carbonation while the top curve corresponds to the shrinkage of a sample undergoing accelerated carbonation in the carbonation chamber. In the air-conditioned room, a stabilization of shrinkage was observed at this time scale while it significantly increased in the carbonation chamber. The difference between the shrinkage curves after 27 days can thus be attributed to the accelerated carbonation shrinkage.

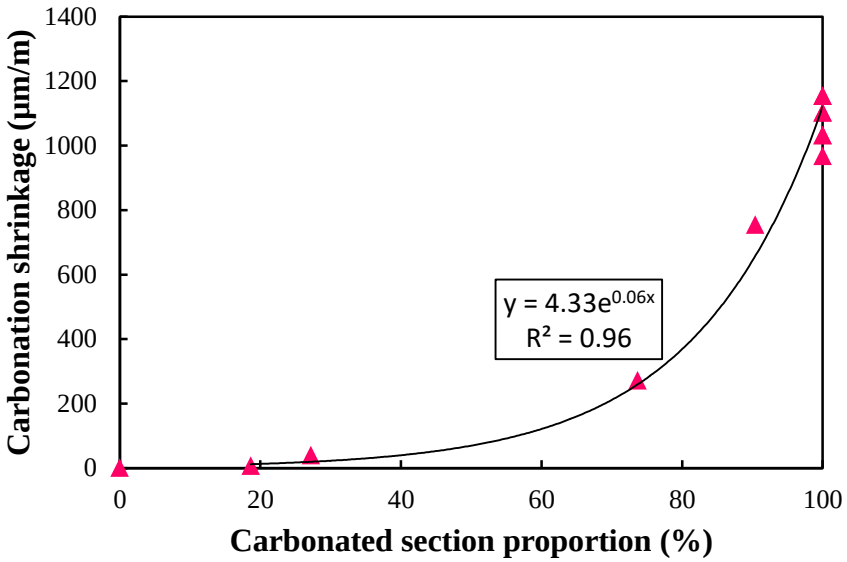

443

444 **Figure 13 : Carbonation shrinkage vs carbonated section proportion**

445 The shrinkage curve showed the same evolution as the carbonated section proportion curve
446 (dotted curve Figure 12). Figure 13 shows the evolution of the carbonation shrinkage as a
447 function of carbonated section proportion. Shrinkage slightly increased at the first day of
448 carbonation when CSP increased from 0 to 20%; a more significant increase of shrinkage was
449 observed for the next few days when CSP increased from 20 to 90%. Then the shrinkage
450 begins to stabilize. As reported in the literature, carbonation shrinkage results from the
451 decalcification and polymerization of C-S-H followed by the formation of amorphous silica
452 gel [26] [29] [51]. The decalcification and polymerization of CSH cause a tension in the
453 carbonated zone. This leads to a differential shrinkage between the surface and the core of the
454 concrete (carbonation shrinkage). These results were recently confirmed in the work of
455 Kangni-Foli [52], that showed on model paste using NMR results, TGA results and
456 carbonation shrinkage measurements that shrinkage increases with the decalcification level of
457 C-S-H. This unambiguously confirms that the shrinkage generated by carbonation is due to
458 decalcification of C-S-H and polymerization of silica chains [52]. Such mechanisms may
459 explain the slight increase in shrinkage at the first day of carbonation given that portlandite

carbonation is dominant compared to that of C-S-H [51]. This large amount of portlandite present at the start of carbonation plays a protective role, it protects C-S-H from carbonation and therefore provides some kind of mechanical protection (decreases carbonation shrinkage) [38]. While the amount of portlandite sharply decreases (Figure 4 and Figure 5) after the first day of carbonation, the carbonation of CSH becomes predominant and results in a significant carbonation shrinkage. After 8 days of carbonation (CR = 90.4%), most of hydration products (especially portlandite and C-S-H) have been carbonated so that the shrinkage begins to stabilize.

It is worth specifying that the shrinkage caused by carbonation (approximatively 1000 μm/m) was significant and reached a value almost equal to drying shrinkage. Such differential shrinkage can cause the development of micro cracks in the carbonated zone as seen in Figure 6-b [26] [28] [53].

3.2.3 Elastic Modulus

The effects of carbonation on the elastic modulus of mortar are shown in Figure 14. The enhancement in elastic modulus with the increase in CSP as observed in Figure 14 [19] [46] [54] leads to a stiffer cement mortar [46]. During accelerated carbonation tests, the hydrated cement matrix is densified and the pore structure is refined due to the precipitation of the formed calcium carbonates [18] [55]. It is also well known that calcium carbonate is an excellent binder [56] providing most of the mechanical resistance of lime mortars [19].

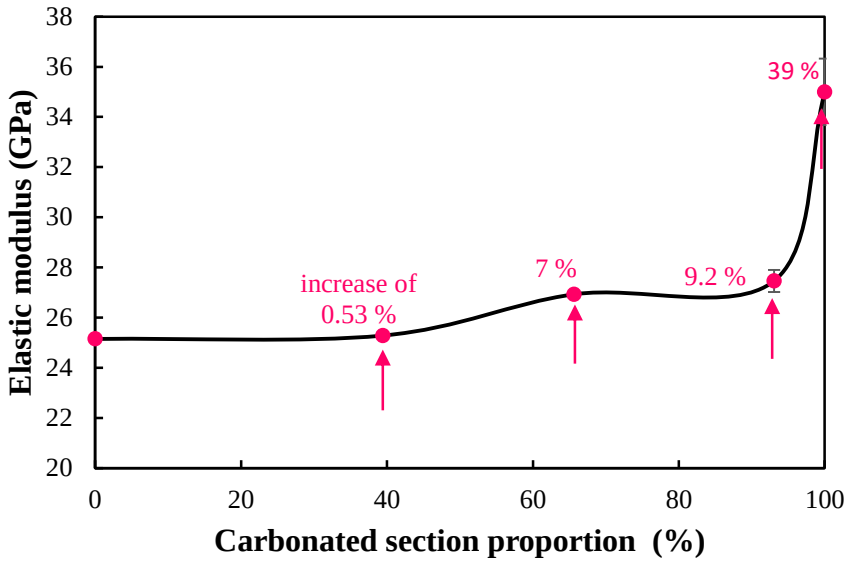

Figure 14 : Elastic modulus of mortar during carbonation

The increase in elastic modulus was not proportional to the carbonation rates [46]. For CSP varying from 0 to 40%, a slight increase of 0.53% was observed. The precipitation of calcium carbonate results in an increase in the volume of the solid phase. At this stage, two zones of different elastic modulus can be present in addition to the transition zone between them. This profile of elastic modulus associated to stresses due to carbonation shrinkage was likely to cause the development of tensile stresses in the external part of the sample. The carbonation actually makes the carbonated zone more prone to cracking [28] [53]. During this first step of carbonation contradictory mechanisms can develop in the cement paste: clogging of the pores and cracking. The tests results suggest that the effects of both mechanisms nearly compensated during this stage: positive effect of calcium carbonate formation ~~as observed in Figure 7~~, and the negative effect of the microcracks, which could explain the limited increase in the modulus of elasticity during the first part of carbonation.

For CSP varying from 40% to 93%, the increase became higher and the elastic modulus reached a value of 27.5 GPa. During the last stage of carbonation in terms of CSP (from 93 to 100%), the elastic modulus reached a value of 35.8 GPa. At this stage the possible cracks

have already developed. At the same time the clogging effect continues, but its rate can be lower for several reasons: the drop in the amounts of carbonatable hydrates, the formation of calcite crystals around the portlandite particles making it difficult to reach it [29] and the decrease in the CO_2 diffusion coefficient after clogging of pores [26]. In this case the clogging not only reduces the volume of the pores but at the same time ensures the healing of microcracks already present or developed during carbonation [57] [58]. In addition, carbonation shrinkage of the inner part of specimens can cause the closure of cracks developed in the outer area. Thus, at this stage, the clogging dominate the cracking effect, moreover the vaterite formed from C-S-H has higher modulus than calcite, which could also explain the significant increase in the elastic modulus of the material at this stage.

3.3 Transport properties

3.3.1 Porosity and pore sizes

Figure 15 shows a decrease in connected open porosity as carbonation progresses. It goes from 23.6% to 19.3% when the CSP increases from 0 to 60%. Such results are expected and they are in agreement with those reported in literature [26] [46] [56] [59] [46]. During carbonation the formation of calcium carbonate causes the clogging of pores and the reduction in total porosity [19] [26] [46]. [25] [60]. This increase in volume depends on the nature of the polymorphic calcium carbonate formed. Houst [19] mentioned that during the carbonation of portlandite if the calcium carbonate precipitates in the form of calcite, an increase of 12% in volume is expected while it is around 19% in the case of formation of vaterite and around 3% in the case of formation of aragonite.

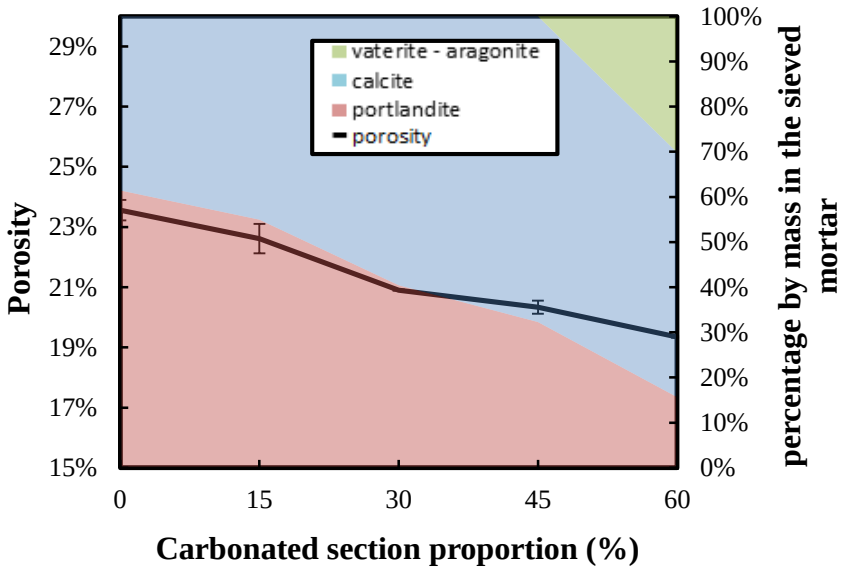

517

518 **Figure 15 : Evolution of the porosity of the mortar during carbonation**

519 More than simply reducing the total porosity, carbonation modifies the pore size distribution.
520 Figure 16 shows the evolution of the pore distribution during carbonation. Three carbonation
521 times were chosen to be characterized: the distribution of pores before carbonation (CSP =
522 0%), after 27 days of carbonation (CSP = 30%) and after 100 days of carbonation (CSP =
523 67%). In these last two cases (CSP = 30% and CSP = 67%) the sample was taken from the
524 carbonated zone.

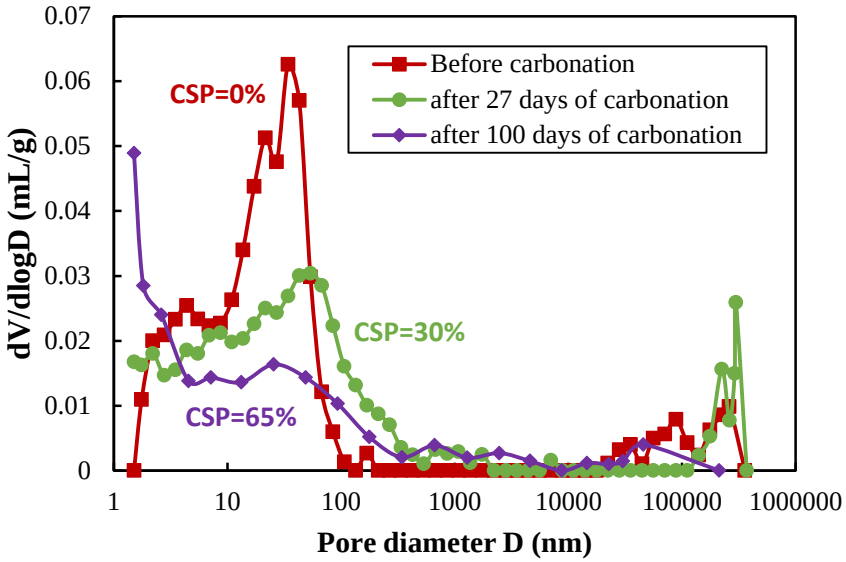

525

526 **Figure 16 : Impact of carbonation on the pore size distribution**

527 The results obtained by mercury porosimetry reveal a decrease in the volume of the
528 mesopores with an access diameter D <50 nm. This decrease can be attributed to the
529 formation of calcium carbonate in the pores during carbonation. The formation of a
530 macroporosity (50 nm < D< 550 nm and D > 22000 nm) can be also distinguished. This
531 increase in the macroporosity could be explained by two phenomena:

532 - The formation of microcracks in the carbonated zone which becomes more brittle and
533 subjected to stress development during carbonation (section 3.1.2). These microcracks
534 result from the carbonation shrinkage and the tensile stresses developed between the
535 carbonated and non-carbonated zone [19] [29].
536 - The structure of the silica gel resulting from the carbonation of the C-S-H. The
537 porosity of silica gel being around 100 nm could therefore be at the origin of
538 macroporosity formation identified [29] [61].

539 This macroporosity was higher in the sample carbonated for 27 days (CSP = 30%) than in the
540 sample carbonated for 100 days. During the first stages of carbonation, several phenomena
541 contribute to the significant formation of macropores. Then, after the progress of carbonation,

the precipitation of calcium carbonate begins to dominate and leads to the healing of cracks. In addition, carbonation shrinkage of the inner area of the cross section can cause the closure of cracks developed in the exterior area and hence the closing of the macropores.

3.3.2 Gas permeability

Figure 17 presents the evolution of the gas permeability during carbonation. Three values of intrinsic permeability were determined for each CSP considered: permeability after 7 days of drying at 80°C (K7), permeability after 28 days of drying at 80°C (K28) and permeability after a total drying at 105°C (Kdry).

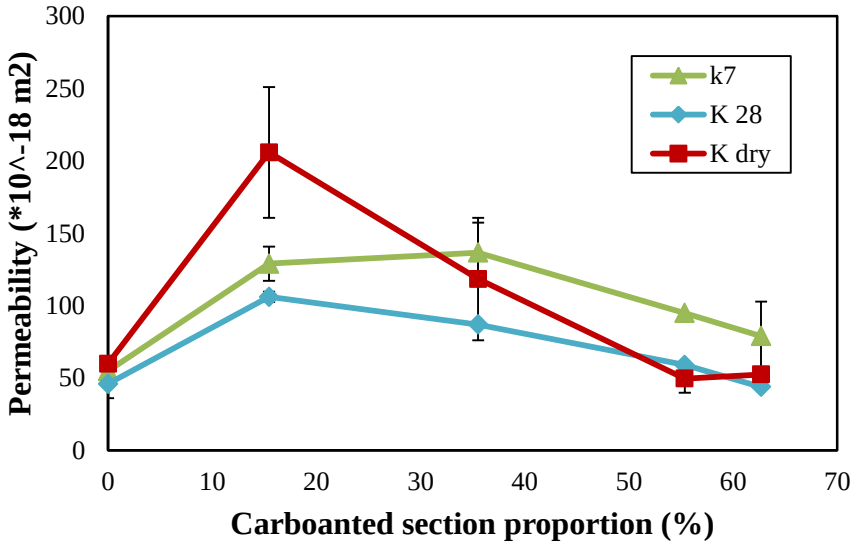

Figure 17 : Evolution of permeability during carbonation

The evolution of permeability with CSP is mostly similar for the three curves considered in this study with a slight shift of the maximum towards lower CSP with specimens drying. An increase in the gas permeability could be observed at the initial stage of carbonation although the total porosity continuously decreased (Figure 15). Such increase has also been observed by Pham et al in 2013 [46] and Thiery in 2005 [26]. The carbonation shrinkage, the tensile stresses and the increase in hardness makes the carbonated zone more prone to cracking [28] [53]. These cracks and microcracks could contribute to the development of macropores as

pointed out by mercury intrusion porosimetry, and together they explain the increase in gas permeability obtained in this first stage of carbonation [26] [46].

Then, as the carbonation progressed, the permeability decreased. This change observed in the evolution of permeability (increases then decreases) is original. The observed decrease in permeability shows the dominant effect of pore-clogging and decrease in porosity. This step began when a significant part of the surface was carbonated. At this stage the carbonation shrinkage has started to stabilize and the gradients of properties across the different zones attenuates leading to the reduction of the tensile stresses. At the same time the clogging of the pores and the closure of microcracks continue ~~. In this case the clogging not only reduces the volume of the pores but at the same time ensures ensuring the healing of microcracks already present or developed during carbonation. In addition, carbonation shrinkage of the inner zone of the cross-section causes the closure of cracks developed in the outer zone and thus the closing of the macropores as observed after 100 days of carbonation in previous section. This induces~~ and consequently induce a decrease in the permeability of the material. Figure 18 summarizes the different mechanisms that take place during the two identified stages of carbonation.

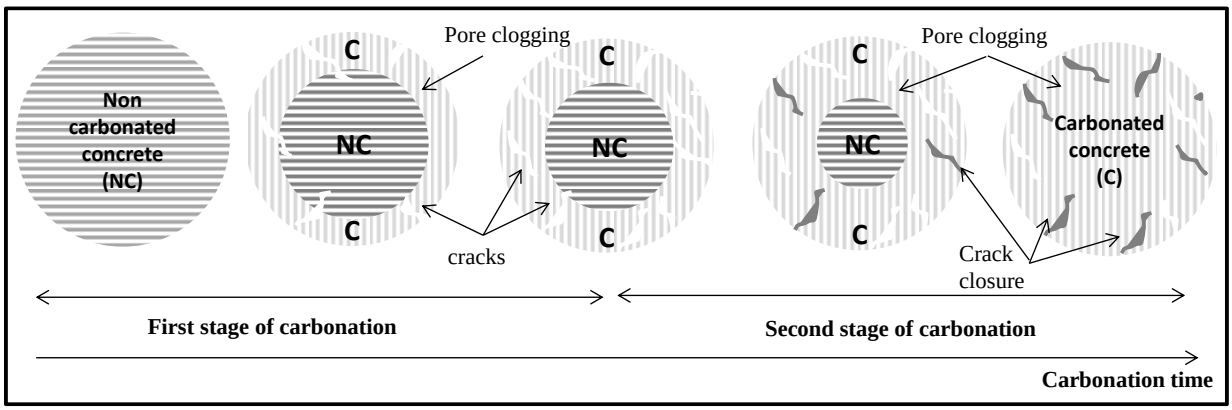

Figure 18 : Schematic drawing of the different stages of carbonation

4 Conclusion

The adhesive old mortar on recycled concrete aggregates seriously affects their properties and therefore the behavior of recycled aggregate concrete. Revealing the variation in the microstructure and transport properties of cement mortars subjected to an accelerated carbonation treatment through a multiscale investigation allows understanding the effects of carbonation on recycled aggregates made with cement-based materials and consequently on the behavior and durability of resulting concrete. From the experimental results and discussion above, the following conclusions can be drawn:

- During the first stage, the carbonation of portlandite dominates leading, in a basic medium, to the precipitation of calcite which is the stable polymorph of calcium carbonate. As the carbonation progresses the portlandite is depleted, and therefore the pH of the concrete decreases, the carbonation of C-S-H begins to prevail leading to the precipitation of unstable polymorphs of $CaCO_3$ (aragonite and vaterite). ~~such as vaterite~~.
- The ~~variations of porosity and~~ evolution of mechanical properties during carbonation depends on the nature of the precipitated polymorph of calcium carbonate. The formation of vaterite during the last stage of carbonation results in a significant increase of elastic modulus both at local and macroscopic scales.
- The carbonation shrinkage developed during accelerated carbonation is significant. Carbonation shrinkage and tensile stresses developed during accelerated carbonation are likely to cause significant damage and cracking, as evidenced by permeability data.
- Two main stages are present at the material scale. During the first phase, contradictory mechanisms develop in the cement paste: clogging of the pores and cracking. The experimental data show that the effects of these two mechanisms nearly compensate in

terms of macroscopic elastic modulus but they induce an increase in permeability at the start of carbonation.

- The second stage begins when most of the surface is carbonated. At this stage, pore clogging and microcracks closing dominates cracking. This explains the improvement observed in the elastic modulus and the continuous reduction in the total porosity accessible to water and permeability of the material.

Acknowledgements

The financial support from Ecole Centrale de Nantes through the PhD thesis grant of Mrs Farah Kaddah is gratefully acknowledged.

References

[1] C.-S. Poon and D. Chan, "The use of recycled aggregate in concrete in Hong Kong," Resources, Conservation and Recycling, p. 13, 2007.
[2] C. Liang, N. Lu, H. Ma, Z. Ma, and Z. Duan, "Carbonation behavior of recycled concrete with CO2-curing recycled aggregate under various environments," Journal of CO_2 Utilization., p. 101185, Jul. 2020.
[3] D. Kong, T. Lei, J. Zheng, C. Ma, J. Jiang, and J. Jiang, "Effect and mechanism of surface-coating pozzalanics materials around aggregate on properties and ITZ microstructure of recycled aggregate concrete," Construction and Building Materials, p. 8, 2010.
[4] P. Belin, G. Habert, M. Thiery, and N. Roussel, "Cement paste content and water absorption of recycled concrete coarse aggregates," Materials and Structures, pp. 1451–1465, Sep. 2014.
[5] D. Xuan, "Assessment of mechanical properties of concrete incorporating carbonated recycled concrete aggregates," Cement and Concrete Composites, p. 8, 2016.
[6] A. Z. Bendimerad, E. Roziere, and A. Loukili, "Combined experimental methods to assess absorption rate of natural and recycled aggregates," Materials and Structures, pp. 3557–3569, Nov. 2015.
[7] K. McNeil and T. H.-K. Kang, "Recycled Concrete Aggregates: A Review," International Journal of Concrete Structures and Materials, pp. 61–69, Mar. 2013
[8] J. Zhang, C. Shi, Y. Li, X. Pan, C.-S. Poon, and Z. Xie, "Influence of carbonated recycled concrete aggregate on properties of cement mortar," Construction and Building Materials, pp. 1–7, Nov. 2015.
[9] C. S. Poon, Z. H. Shui, and L. Lam, "Effect of microstructure of ITZ on compressive strength of concrete prepared with recycled aggregates," Construction and Building Materials., pp. 461–468, Jul. 2004.

[10] N. Lippiatt, T.-C. Ling, and S.-Y. Pan, "Towards carbon-neutral construction materials: Carbonation of cement-based materials and the future perspective," Journal of Building Engineering, p. 101062, Mar. 2020.
[11] J. Pacheco and J. de Brito, "Recycled aggregates produced from construction and demolition waste for structural concrete: constituents, properties and production," Materials, p. 5748, Oct. 2021.
[12] R. V. Silva, J. de Brito, and R. K. Dhir, "Use of recycled aggregates arising from construction and demolition waste in new construction applications," Journal of Cleaner Production, p. 117629, Nov. 2019.
[13] S. Jayakody, A. M. Z. Zimar, and R. A. L. M. Ranaweera, "Potential use of recycled construction and demolition waste aggregates for non- structural concrete applications" Journal of the National Science Foundation of Sri Lanka p. 205, Jun. 2018.
[14] V. W. Y. Tam, C. M. Tam, and K. N. Le, "Removal of cement mortar remains from recycled aggregate using pre-soaking approaches," Resources, Conservation and Recycling, pp. 82–101, Mar. 2007.
[15] B. Zhan, C. S. Poon, Q. Liu, S. Kou, and C. Shi, "Experimental study on CO_2 curing for enhancement of recycled aggregate properties," Construction and Building Materials, pp. 3–7, Sep. 2014.
[16] S.-C. Kou, B. Zhan, and C.-S. Poon, "Use of a CO_2 curing step to improve the properties of concrete prepared with recycled aggregates," Cement and Concrete Composites, pp. 22–28, Jan. 2014.
[17] S. K. Kaliyavaradhan, T.-C. Ling, and K. H. Mo, "CO2 sequestration of fresh concrete slurry waste: Optimization of CO2 uptake and feasible use as a potential cement binder" Journal of CO_2 Utilization, p. 101330, Dec. 2020.
[18] J. Zhan, "Carbonation treatment of recycled concrete aggregate_ Effect on transport properties and steel corrosion of recycled aggregate concrete," Cement and Concrete Composites, p. 8, 2019.
[19] Y. F. Houst and F. H. Wittmann, "Retrait de carbonatation," Ein Dienst der ETH-Bibliothek, p. 255, 1989.
[20] C. Pade and M. Guimaraes, "The CO_2 uptake of concrete in a 100 year perspective," Cement and Concrete Research., p. 9, 2007.
[21] M. Sereng, "Improvement of the properties of recycled aggregates by CO2 storage: pre-industrial feasibility study," University of Paris-Est, France, 2020, PhD thesis.
[22] J. Zhang, C. Shi, Y. Li, X. Pan, C.-S. Poon, and Z. Xie, "Performance enhancement of recycled concrete aggregates through carbonation," Journal of Materials in Civil engineering, p. 04015029, Nov. 2015.
[23] D. Wang, T. Noguchi, and T. Nozaki, "Increasing efficiency of carbon dioxide sequestration through high temperature carbonation of cement-based materials," Journal of Cleaner Production, p. 117980, Nov. 2019.
[24] G. Pan, M. Zhan, M. Fu , Y. Wang, X. Lu "Effect of CO2 curing on demolition recycled fine aggregates enhanced by calcium hydroxide pre-soaking," Construction and Building Materials, p. 9, 2017.
[25] Y. F. Houst, "The role of moisture in the carbonation of cementitious materials," Internationale Zeitschrift für, p. 18, 1996.
[26] M. Thiery, " Modeling of atmospheric carbonation of cementitious materials: Consideration of kinetic effects and microstructural and water modifications" Ecole nationale des ponts et chaussées, France, 2007, PhD thesis
[27] J. Han, W. Sun, G. Pan, and W. Caihui, "Monitoring the evolution of accelerated carbonation of hardened cement pastes by X-Ray computed tomography," Journal of Materials in Civil Engineering, pp. 347–354, 2013.

[28] D. Cui, X. Zuo, K. Zheng, and S. Talukdar, “Tomography-based investigation on the carbonation behavior through the surface-opening cracks of sliced paste specimen” materials, p. 17, 2020.
[29] E. Drouet, “ Impact of temperature on the carbonation of cementitious materials: consideration of water transfers” Ecole normale supérieure de Cachan, France, 2011, PhD thesis.
[30] R. E. Hachem, “ Multicriteria study of the degradation of cementitious materials by external sulphate attack” Ecole Centrale de Nantes, France, 2010, PhD thesis.
[32] M. Khachani, A. E. Hamidi, M. Halim, and S. Arsalane, “Non-isothermal kinetic and thermodynamic studies of the dehydroxylation process of synthetic calcium hydroxide Ca(OH)2,” Journal of Materials and Environmental Science, p. 11, 2014.
[33] G. Villain, M. Thiery, and G. Platret, “Measurement methods of carbonation profiles in concrete: Thermogravimetry, chemical analysis and gammadensimetry,” Cement and Concrete Research, pp. 1182–1192, Aug. 2007.
[34] A. Morandeau, “Investigation of the carbonation mechanism of CH and C-S-H in terms of kinetics, microstructure changes and moisture properties,” Cement and Concrete Research, p. 18, 2014.
[35] E. Rozière, A. Loukili, and F. Cussigh, “A performance based approach for durability of concrete exposed to carbonation,” Construction and Building Materials ,pp. 190–199, Jan. 2009.
[36] G. S. dos Reis, B. G. Cazacliu, R. Artoni, and J. Torrenti, “Effect of the accelerated carbonation treatment on the recycled sand physicochemical characteristics through the rolling carbonation process,” Journal of CO_2 Utilization., p. 101181, Jul. 2020.
[37] Y. Pu, L. Li, Q. Wang, X. Shi, L. Fu, G. Zhang, C. Luan, A. Abomohra, “Accelerated carbonation treatment of recycled concrete aggregates using flue gas: A comparative study towards performance improvement,” Journal of CO_2 Utilization, p. 101362, Jan. 2021.
[38] Y. Li et al., “Carbonation of the synthetic calcium silicate hydrate (C-S-H) under different concentrations of CO2: Chemical phases analysis and kinetics,” Journal of CO2 Utilization., pp. 303–313, Jan. 2020.
[39] J. Grandet, “Contribution to the study of the setting and carbonation of mortars in contact with porous materials " Universiy of Paul Sabatier Toulouse, France, 1975, PhD thesis
[40] J. Chang, D. Wang, and Y. Fang, “Effects of mineralogical changes in BOFS during carbonation on pH and Ca and Si leaching,” Construction and Building Materials, pp. 584–592, Dec. 2018.
[41] Ç. Oral, “Influence of pH on morphology, size and polymorph of room temperature synthesized calcium carbonate particles,” Powder Technology., p. 8, 2018.
[42] B. Kammoe and R. Brice, “Synthèse de nanoparticules de carbonate de calcium,” p. 92.
[43] R. SevIk, “Physical and nanomechanical properties of the synthetic anhydrous crystalline $CaCO_3$ polymorphs: vaterite, aragonite and calcite”, J Mater Sci, 2018.
[44] H. Nebel and M. Epple, “Continuous preparation of calcite, aragonite and vaterite, and of magnesium-substituted amorphous calcium carbonate (Mg-ACC),” Z. Für Anorg. Allg. Chem., pp. 1439–1443, Jul. 2008.
[45] D. Xuan, B. Zhan, and C. S. Poon, “Assessment of mechanical properties of concrete incorporating carbonated recycled concrete aggregates,” Cement and Concrete Composites, pp. 67–74, Jan. 2016.

[46] S. T. Pham, “Modifications on microporosity and physical properties of cement mortar caused by carbonation: comparison of experimental methods,” Hindawi Publishing Corporation, p. 10, 2013.
[47] M. Auroy, “Impact of carbonation on unsaturated water transport properties of cement-based materials” Cement and Concrete Research ,p. 288, 2015.
[48] N. Hyvert, “Application of the probabilistic approach to the durability of precast concrete products” University of Toulouse, France, 2009 PhD thesis.
[49] S. T. Pham, “Modifications in water sorption isotherms of cement mortars caused by carbonation: effects of cycles,” Advanced Materials Research., pp. 3–9, Oct. 2014.
[50] H. Jiande, S. Wei, P. Ganghua, W. Caihui, and R. Hui, “Application of X-ray computed tomography in characterization microstructure changes of cement pastes in carbonation process,” Journal of Wuhan University of Technology-Mater Sci Ed, p. 7, April 2012.
[51] J. J. Chen, J. J. Thomas, and H. M. Jennings, “Decalcification shrinkage of cement paste,” Cement and Concrete Research, pp. 801–809, May 2006.
[52] E. Kangni-Foli, S. Poyet, P. Le Bescop, T. Charpentier, F. Bernachy-Barbé, A. Dauzères, E. L’Hopital a, J.-B. d’Espinose de Lacaillerie, “Carbonation of model cement pastes: The mineralogical origin of microstructural changes and shrinkage,” Cement and Concrete Research., p. 106446, Jun. 2021.
[53] H. Jiande, S. Wei, P. Ganghua, W. Caihui, and R. Hui, “Application of X-ray Computed Tomography in characterization microstructure changes of cement pastes in carbonation process,” Journal of Wuhan University of Technology-Mater Sci Ed, p. 7, April 2012.
[54] C.-F. Chang, “Strength and elastic modulus of carbonated concrete.”, ACI materials journal, 2005
[55] C. A. Garcıa-Gonzalez, A. Hidalgo, C. Andrade, M. Cruz Alonso, J. Fraile, A. M. Lopez-Periago, and C.´n Domingo, “Modification of composition and microstructure of portland cement pastes as a result of natural and supercritical carbonation procedures,” Industrial & Engineering Chemistry Research, p. 8, 2006.
[56] A. Younsi, “ Carbonation of concretes with high rates of substitution of cement by mineral additions,” University of La Rochelle, France, 2012, PhD thesis.
[57] T. Danner and M. R. Geiker, “Long-term Influence of concrete surface and crack orientation on self-healing and ingress in cracks – Field Observations,” Nordic Concrete Research, pp. 1–16, Jun. 2018.
[58] Carola Edvardsen, “Water permeability and autogenous healing of cracks in concrete,” ACI materials journal, Jan. 1999.
[59] B. A. Silva, A. P. Ferreira Pinto, A. Gomes, and A. Candeias, “Effects of natural and accelerated carbonation on the properties of lime-based materials,” Journal of CO_2 Utilization.,p. 101552, Jul. 2021.
[60] V. T. Ngala and C. L. Page, “Effects of carbonation on pore structure and diffusional properties of hydrated cement pastes” Cement and Concrete Research., pp. 995–1007, Jul. 1997.
[61] T. A. Bier, “Influence of type of cement and curing on carbonation progress and pore structure of hydrated cement pastes,” 1987.